

Journal of Intelligent Material Systems and Structures

<http://jim.sagepub.com/>

Modeling of a distributed device for simultaneous reactive vibration suppression and energy harvesting

Ryan L Harne and Chris R Fuller

Journal of Intelligent Material Systems and Structures 2012 23: 655 originally published online 21 February 2012

DOI: 10.1177/1045389X12436736

The online version of this article can be found at:

<http://jim.sagepub.com/content/23/6/655>

Published by:



<http://www.sagepublications.com>

Additional services and information for *Journal of Intelligent Material Systems and Structures* can be found at:

Email Alerts: <http://jim.sagepub.com/cgi/alerts>

Subscriptions: <http://jim.sagepub.com/subscriptions>

Reprints: <http://www.sagepub.com/journalsReprints.nav>

Permissions: <http://www.sagepub.com/journalsPermissions.nav>

Citations: <http://jim.sagepub.com/content/23/6/655.refs.html>


>> [Version of Record](#) - Apr 9, 2012

[OnlineFirst Version of Record](#) - Feb 21, 2012

[What is This?](#)

Modeling of a distributed device for simultaneous reactive vibration suppression and energy harvesting

Ryan L Harne and Chris R Fuller

Journal of Intelligent Material Systems and Structures
23(6) 655–664
© The Author(s) 2012
Reprints and permissions:
sagepub.co.uk/journalsPermissions.nav
DOI: 10.1177/1045389X12436736
jim.sagepub.com


Abstract

Distributed devices or treatments are a mainstay of passively suppressing structural vibrations. In some cases, piezoelectric materials were included within the devices to utilize them as actuators. Interest in energy harvesting encourages a reassessment of these devices, using the piezoelectric materials as a means to convert input vibrational energy into electrical power. A numerical model of one such device, exhibiting mass-spring-damper dynamics, attached to a vibrating host structure is described and validated against 3D finite element analysis. The model is utilized to evaluate the simultaneous goals of passive vibration attenuation and energy harvesting of devices on a lightweight, clamped panel. The objectives are found to be partly in opposition, particularly when the total mass of the added devices becomes more substantial. This feature is widely neglected in employing mass-spring systems as energy-harvesting devices, where the mass of the device is insubstantial relative to the main structure. As a result, compromises or alternatives may be explored to achieve both goals: the implementation of materials exhibiting greater electromechanical coupling, minimization of total applied mass to the host structure, and retuning of attached devices to exhibit natural frequencies not exactly equal to those of the host structure.

Keywords

energy harvesting, piezoelectric, structural health monitoring, vibration control

Introduction

The interest in converting ambient vibrational energy into a useful electrical power source has fostered a range of practical implementations and numerical modeling strategies. In many embodiments, the devices employ dynamics identical to traditional mass-spring-dampers (vibration absorbers) historically used for passive and active vibration control purposes.

Due to the significant in-phase strains possible, cantilevered beams designed to operate at the first modal frequency are often employed, in tandem with attached piezoelectric or piezoceramic layers. Devices described or studied by Roundy and Wright (2004), Lefeuvre et al. (2006), and Erturk et al. (2009) have shown an appreciable potential in converting vibrational energy into usable power. Though it is of little or no interest in energy-harvesting applications, in the case of cantilevered beam harvesters, the beams supply a reactive bending moment back to the host structure. With a contrasting focus, cantilever beam vibration absorbers utilize this bending moment to suppress the vibration of their host structure (Jacquot and Foster, 1977). The gap between employing a cantilevered beam as an

energy-harvesting device and as a vibration control device exists between the assumption of relative inertial influence: energy-harvesting devices tend to be of little or effectively no mass compared to the host structure (e.g. harvester on a bridge), whereas the vibration control device is more substantial (e.g. mass-spring-damper on an aircraft panel).

The disparity between the fields of vibration control and energy harvesting is apparent in the modeling methodology. In a fundamental analysis, vibration control studies consider two- or multidegree-of-freedom systems (Den Hartog, 1985); in energy harvesting, a single-degree-of-freedom (SDOF) system with base excitation is evaluated (Stephen, 2006). Thus, it is presumed, in a large proportion of energy-harvesting

Vibration and Acoustics Laboratories, Department of Mechanical Engineering, Virginia Polytechnic Institute and State University, Blacksburg, VA, USA

Corresponding author:

Ryan L Harne, Vibration and Acoustics Laboratories, Department of Mechanical Engineering, Virginia Polytechnic Institute and State University, 131 Durham Hall (MC 0238), Blacksburg, VA 24061, USA.
Email: rharne@vt.edu

studies, that the harvester does not affect the vibration of the greater host structure to which it will ultimately be attached.

With a growing interest in power harvesting has come the desire to convert ambient vibration from a broad array of sources. Yet, in some of these cases, it may no longer be appropriate to assume the attached devices are a negligible inertial influence to the host structure, for instance, a harvester on a lightweight aircraft panel. Thus, a new analysis must be made for devices employing energy-harvesting technology that may also modify the vibrational response of the host structure or devices generally intended for the simultaneous purposes of vibration suppression and power harvesting.

To avoid confusion, a note should be made regarding the use of the phrase “simultaneous vibration suppression and energy harvesting.” Elsewhere in literature, this concept appears in regards to the damping and stiffening effects of the external load resistance across a piezoelectric electrode as the harvester oscillates (Lesieutre et al., 2004; Liang and Liao, 2009). The observed damping effects are primarily considered to be affecting the harvester itself—for example, the bimorph cantilevered beam dynamics—as opposed to the structural dynamics of a larger system. This justifies the implicit modeling assumption that the device is excited by base vibration or a unit force (i.e. an infinite energy source).

In the present analysis, the base structure, that is, a structural panel, is externally excited and harvesters, in the form of mass-spring systems, are thereafter attached. The piezoelectric materials are not fully attached to the host structure but are contained within some manifestation of a distributed spring layer. Thus, the vibration-suppression effect is due to the attached devices reactively or resistively working against the motion of the host structure. One similar embodiment of this design appears in the literature in the event that the cantilever beam harvesters are the wings of an aircraft (De Marqui et al., 2010). The present work is distinguished from the prior in that the harvester devices exhibit reactive and resistive dynamics as opposed to only resistive. In other words, the present harvester designs of interest work against the host structure by reactive forces like vibration absorbers as well as resist the structural vibration like constraining treatments.

A passive vibration control device is considered, termed smart foam by Gentry et al. (1997), which utilizes a distributed poroelastic spring layer in which a curvature of piezoelectric film is embedded. Smart foam was intended to serve as a combined passive and active acoustic-structural device and was successfully employed in active noise control experiments (Guigou and Fuller, 1999; Leroy et al., 2011). Marcotte et al. (1999) studied this device with the addition of a distributed top mass layer, the resulting embodiment then combining passive

vibration absorber dynamics alongside the potential of active control. In the context of energy harvesting and passive vibration control, the smart foam design is considered in that it may not only reactively suppress the vibrations of the host structure but also generate electrical power as the embedded piezoelectric film is strained within the deformed spring layer.

This article briefly describes an analytical model based on the generalized Hamilton’s principle of a distributed device, like smart foam, when applied to an excited, vibrating structure. The model is validated by comparison with the results from 3D finite element (FE) analysis and is found to be much more computationally efficient to solve as compared with FE analysis. The model is then employed to consider the simultaneous capability of smart foam samples to reduce vibration levels of a lightweight, clamped panel as well as to harvest electrical energy. Though the simultaneous objectives are not mutually exclusive, potential tradeoffs exist and are discussed.

Model formulation

Mechanical domain description

For conciseness and to focus primarily on the results of the model simulations, only essential elements of the present variational formulation are provided. Greater detail on the generalized Hamilton’s principle is available in a number of texts (Meirovitch, 1967; Reddy, 1984) as well as a recent, similar derivation of this variational method for energy harvesting using piezoelectric plates in the context of the FE method (De Marqui et al., 2009).

Consider a system composed of a base plate to which one or more piezoelectric vibration control devices are attached, Figure 1. The attached devices are each composed of a distributed spring layer and a distributed top plate; the spring layer itself is a composite of a continuous material and a piezoelectric layer. In the following

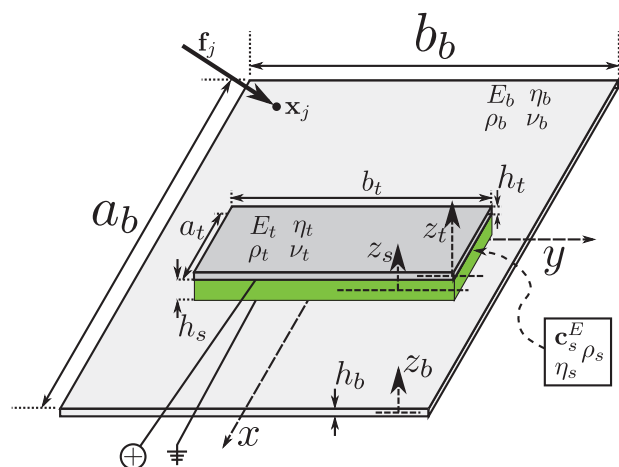


Figure 1. Geometry and material properties of the model.

analysis, subscripts b, s, p , and t refer to the base plate, the distributed spring layer, the embedded piezoelectric layer, and the distributed top plate, respectively. The origin of the global coordinate system is defined at the center point of base plate and the (x, y) plane corresponds to the middle plane of the base plate, $z_b = 0$. The base plate is arbitrarily bounded and may be excited by a number of localized point forces, $\mathbf{f}_j(\mathbf{x}_j)$.

The base plate and distributed top plate are assumed to be Love–Kirchhoff plates having displacements expressed in the form

$$\mathbf{u}(\mathbf{x}, t)_{i=b,t} = \begin{bmatrix} u_{io}(x, y, t) - z_i \frac{\partial w_{io}(x, y, t)}{\partial x} \\ v_{io}(x, y, t) - z_i \frac{\partial w_{io}(x, y, t)}{\partial y} \\ w_{io}(x, y, t) \end{bmatrix} \quad (1)$$

where the second subscript o indicates the displacement in the middle plane of the plate, $z_b = 0$ or $z_t = 0$.

For simplification of the analysis, the distributed spring layer is approximated as a superposition of a thick, transversely deformable, orthotropic plate and a thin, cylindrical shell, which exhibits piezoelectric properties (see Figure 2). The mechanical displacements of the thick orthotropic plate allow for the transverse flexibility of the layer

$$\mathbf{u}(\mathbf{x}, t)_s = \begin{bmatrix} u_{so}(x, y, t) + z_s \theta_x(x, y, t) \\ v_{so}(x, y, t) + z_s \theta_y(x, y, t) \\ w_{so}(x, y, t) + z_s \frac{\partial w_{so}(x, y, t)}{\partial z_s} + \frac{1}{2} z_s^2 \frac{\partial^2 w_{so}(x, y, t)}{\partial z_s^2} \end{bmatrix} \quad (2)$$

where θ_x and θ_y are the rotations about the middle planes in the x -axis and y -axis, respectively. Application of continuity of displacements and transverse stress between the spring layer and the two bounding plates allows the spring layer mechanical displacements to be expressed in terms of the displacements of the top plate and bottom plate

$$\mathbf{u}(\mathbf{x}, t)_s = \begin{bmatrix} \frac{1}{2} [u_{to} + u_{bo}] + \frac{1}{4} \left[h_t \frac{\partial w_{to}}{\partial x} - h_b \frac{\partial w_{bo}}{\partial x} \right] + \frac{1}{h_s} z_s \left\{ [u_{to} - u_{bo}] + \frac{1}{2} \left[h_t \frac{\partial w_{to}}{\partial x} + h_b \frac{\partial w_{bo}}{\partial x} \right] \right\} \\ \frac{1}{2} [v_{to} + v_{bo}] + \frac{1}{4} \left[h_t \frac{\partial w_{to}}{\partial y} - h_b \frac{\partial w_{bo}}{\partial y} \right] + \frac{1}{h_s} z_s \left\{ [v_{to} - v_{bo}] + \frac{1}{2} \left[h_t \frac{\partial w_{to}}{\partial y} + h_b \frac{\partial w_{bo}}{\partial y} \right] \right\} \\ \frac{1}{2} [w_{to} + w_{bo}] + \frac{1}{h_s} z_s [w_{to} - w_{bo}] \end{bmatrix} \quad (3)$$

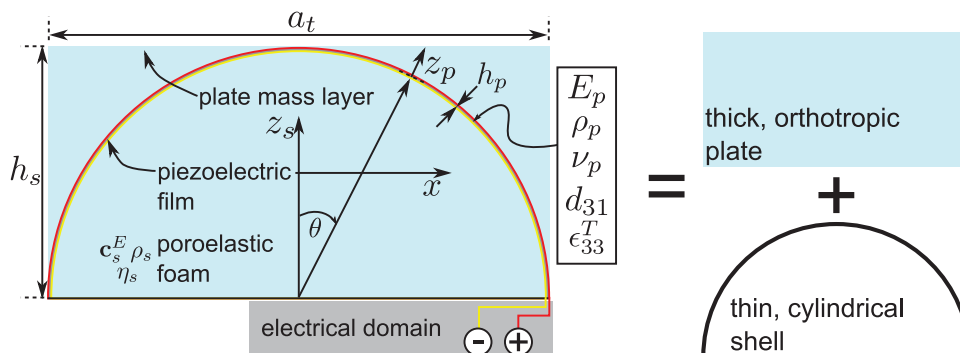


Figure 2. Layout of distributed spring layer, the superposition of a thick plate and thin shell.

It is assumed that the inertial influence of the shell is negligible compared to the host spring layer material; in practice, the piezoelectric film may constitute 5% or less of the mass of the whole spring layer. Following this assumption, the displacements of the embedded piezoelectric film correspond to those of the thick orthotropic plate, evaluated over the surface defined by the film. This assumption would not be valid, however, in the event that the embedded piezoelectric material was more substantial relative to the host spring layer. In the latter case, rather than assumptions of superposition, it may be more appropriate to determine equivalent elasticity characteristics of the full spring layer using homogenization or experimental techniques (Bakhvalov and Panasenko, 1989; Jaouen et al., 2008).

In this manner, for n attached vibration control and energy-harvesting devices, the coupled system mechanical displacements constitute $3 + 3n$ unknowns: u_{bo}, v_{bo} , and w_{bo} for the base structure and u_{to}, v_{to} , and w_{to} for each device.

Electrical domain description

In the present analysis, the following assumptions are taken: (1) continuous electrodes cover the top and bottom surfaces of each piezoelectric domain; (2) the piezoelectric materials are poled in the thickness direction, z_p ; and (3) the only nonzero electric field component varies linearly through the thickness of the material. As a result of assumption (1), only one voltage is necessary to describe the electrical response of each piezoelectric domain.

In the following study, smart foam samples containing a single half-circular segment of embedded piezoelectric film are considered. A simple means by which to increase the collective output of voltage is to utilize a multitude of periods of the film and connect the individual voltage outputs in series. Figure 3 shows an

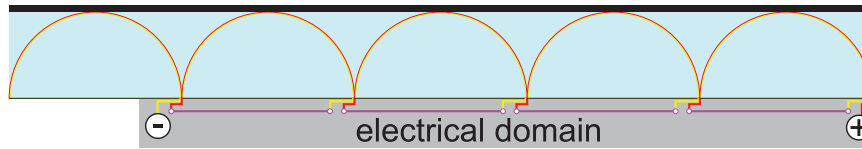


Figure 3. Smart foam sample containing a periodic embedded piezoelectric film for improving voltage output, showing voltages added in series.

example implementation of this design. Furthermore, other embedded shapes of piezoelectric material may be employed, which may be more effective in converting the transmitted strain to electrical energy.

Approximate solution

The mechanical displacements and voltages are estimated to be the linear combination of admissible trial functions and generalized coordinates

$$\mathbf{u}(\mathbf{x}, t)_{i=b,t} = (\Psi_m(\mathbf{x})\mathbf{m}(t))_i \quad (4)$$

$$\mathbf{v}(\mathbf{x}, t) = \Psi_v(\mathbf{x})\mathbf{z}(t) \quad (5)$$

where $\Psi_m(\mathbf{x})$ and $\Psi_v(\mathbf{x})$ are the admissible trial functions and $\mathbf{m}(t)$ and $\mathbf{z}(t)$ are the generalized coordinates for the mechanical and electrical domains, respectively. The generalized coordinates and trial functions number N_b and N_t for the base and top plates, respectively. Given the assumptions of continuous electrodes covering the top and bottom surfaces of the piezoelectric material, it is convenient to represent the generalized electrical coordinate as a single parameter, $z(t)$.

Substituting these solutions into the generalized Hamilton's principle, assuming an harmonic time dependence of the form $e^{i\omega t}$, and assuming there is no external electrical excitation on the piezoelectric electrodes, yields a coupled systems of equations describing the mechanical and electrical response for a passive vibration control and/or energy-harvesting device attached to an excited host structure (De Marqui et al., 2009)

$$\begin{bmatrix} Y^c + j\omega C_p & j\omega\Theta^t \\ -\Theta & \mathbf{K} + j\omega\mathbf{C} - \omega^2\mathbf{M} \end{bmatrix} \begin{bmatrix} z \\ \mathbf{m} \end{bmatrix} = \begin{bmatrix} 0 \\ \mathbf{F} \end{bmatrix} \quad (6)$$

where the components of equation (6) are provided in Appendix 1. For n attached devices, the coupled system of equations contains $3N_b + 3nN_t$ mechanical generalized coordinates and n electrical generalized coordinates. The attached circuit admittance, Y^c , for energy-harvesting devices is a simple load resistance, $Y^c = 1/R_1$.

The generalized coordinates and electrical responses are computed from equation (6) as

$$\mathbf{m} = [\mathbf{K} + j\omega\mathbf{C} - \omega^2\mathbf{M} + j\omega(Y^c + j\omega C_p)^{-1}\Theta\Theta^t]^{-1}\mathbf{F} \quad (7)$$

$$z = -[Y^c + j\omega C_p]^{-1}(j\omega\Theta^t)$$

$$[\mathbf{K} + j\omega\mathbf{C} - \omega^2\mathbf{M} + j\omega(Y^c + j\omega C_p)^{-1}\Theta\Theta^t]^{-1}\mathbf{F} \quad (8)$$

For a given distributed piezoelectric vibration control and energy-harvesting device, the frequency response function (FRF) of the transverse acceleration of the top plate to that of the transverse acceleration of the base plate is computed as

$$|\text{FRF}_{accel}(\omega)| = \left| \frac{-\omega^2 w_{to}(x_1, y_1, \omega)}{-\omega^2 w_{bo}(x_2, y_2, \omega)} \right| = \left| \frac{\Psi_{m_{w_{to}}}(x_1, y_1)\mathbf{m}_{w_{to}}(\omega)}{\Psi_{m_{w_{bo}}}(x_2, y_2)\mathbf{m}_{w_{bo}}(\omega)} \right| \quad (9)$$

where $\Psi_{m_{w_{to}}}$ and $\mathbf{m}_{w_{to}}$ are the trial functions and generalized coordinates related to the transverse displacement of the top plate, respectively; $\Psi_{m_{w_{bo}}}$ and $\mathbf{m}_{w_{bo}}$ are the trial functions and generalized coordinates related to the transverse displacement of the base plate, respectively; and (x_1, y_1) and (x_2, y_2) are the points of evaluation. The voltage FRF (V g^{-1}) of a device is computed as

$$|\text{FRF}_{volt}(\omega)| = \left| \frac{z(\omega)}{-\omega^2 \Psi_{m_{w_{bo}}}(x_2, y_2)\mathbf{m}_{w_{bo}}(\omega)} \right| \quad (10)$$

Considering the FRF responses in light of equation (7), the mechanical response of the system is damped and shifted in frequency by the specific of circuit admittance and piezoelectric characteristics. The significance of this effect is modulated by the magnitude of the electromechanical coupling terms, Θ . The same frequency shift is observed in the electrical response, but the magnitude of the voltage FRF is predicted to continually increase with increasing R_1 to short circuit conditions.

In considering the vibration attenuation capability of a device on a larger host structure, the mean square out-of-plane velocity ($\text{m}^2 \text{s}^{-2}$) of the base plate is determined by

$$\langle \dot{w}_{bo}(\omega) \rangle^2 = \frac{\omega^2}{8a_b b_b} \int_{-a_b/2}^{+a_b/2} \int_{-b_b/2}^{+b_b/2} \left(\Psi_{m_{w_{bo}}}(x, y)\mathbf{m}_{w_{bo}}(\omega) \right)^* \left(\Psi_{m_{w_{bo}}}(x, y)\mathbf{m}_{w_{bo}}(\omega) \right) dx dy \quad (11)$$

where $()^*$ denotes the complex conjugate. Recalling that the spring layer mechanical displacements were expressed in terms of the bounding displacements of the plate, the transverse generalized coordinates of the base plate, $\mathbf{m}_{w_{bo}}$, contain terms related to the spring layer as well as coupling terms related to the top mass displacements. Furthermore, the electromechanical coupling, Θ ,

is expressed in terms of mechanical displacements of the bounding plates as well as the electrical response itself. As a result, the presence of the piezoelectric spring layer slightly dampens and shifts in frequency the response of the base and top plates to varying degrees as the external load resistance is modified.

Validation against 3D FE solution

The present model is compared against the results computed from a 3D FE model using the COMSOL software package (COMSOL AB, 2007). As was recommended by Leroy et al. (2009), due to the thinness of the embedded piezoelectric film relative to the foam layer, the film is modeled as a 2D surface (shell elements). Acoustic coupling within the poroelastic foam is ignored since vibration-suppression and energy-harvesting capabilities are the metrics of present interest. The poroelastic material is modeled using tetrahedral solid elements, while the base plate is constructed using shell elements. A diagram of the 3D FE mesh is shown in Figure 4, which used approximately 8000 total elements.

A smart foam sample employing the half-circular embedded piezoelectric film shape is centrally located

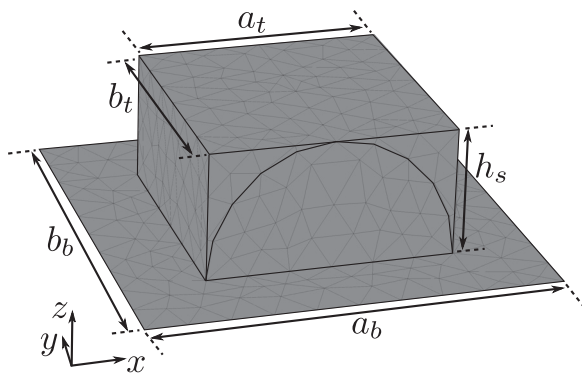


Figure 4. FE model mesh of vibration control and energy-harvesting device.
FE: finite element.

on a base plate having free boundaries. The base plate is excited by a centrally located, out-of-plane, unit harmonic force, $f_z(0, 0, 0, \omega) = 1$ N. Geometric and material properties of the layers are provided in Table 1; properties of the embedded piezoelectric film are provided in Table 2 (Bailo et al., 2003). The base plate is modeled as being exceptionally stiff in order to excite the attached device equally at all frequencies and to avoid modal effects of the base structure within the frequency range of interest. The foam layer is assumed to have identical elastic properties regardless of orientation; that is, $E_x = E_y = E_z = E$ and $G_{yz} = G_{xz} = G_{xy} = E/2(1 + \nu)$. Damping for all layers is included by means of an isotropic loss factor, η . Figure 5 compares the present model predictions of out-of-plane acceleration FRF and those computed by the FE model for three values of load resistance, R_1 . A resonance is evident at 224 Hz, with the FE and present models in perfect agreement of the frequency. This represents the SDOF transverse resonance of the device.

As the load resistance on the electrodes is increased, the SDOF resonance frequency is seen to moderately shift from 224 Hz at $R_1 = 1.8$ k Ω to 225 Hz at $R_1 = 560$ k Ω . In addition to the minor shift in frequency, both the FE model and the present numerical model concur that the amplitude of the resonance increases as load resistances increase; the magnitude increases from 25.4 at $R_1 = 1.8$ k Ω to 33.9 at $R_1 = 560$ k Ω . This is a one-third increase in the magnitude of the resonance (+2.5 dB). This suggests that as a distributed vibration control treatment, different load resistances (in this case, larger resistances) would improve the ability of the device to reactively work against the host structural vibration for this device design.

Voltage FRF predictions are compared in Figure 6 for four values of R_1 . The same resonance effect witnessed in the acceleration FRF is observed for the voltage output, also at 224 Hz but increasing to 225 Hz for $R_1 = 560$ k Ω . For greater load resistances, the increased time constant, $R_1 C_p$, serves to reduce the voltage output at higher frequencies, while the lower frequency

Table 1. Geometric and mechanical properties of the layers.

Layer	a (m)	b (m)	h (mm)	E (Pa)	ν	ρ (kg/m ³)	η
Base	0.10	0.10	5	2.1e14	0.33	7850	3e-4
Top	0.06	0.06	2	7.1e10	0.33	2100	3e-4
Spring layer	0.06	0.06	30	1.9e5	0.4	9	4e-2

Table 2. Mechanical and electrical characteristics of the embedded piezoelectric film.

h_p (m)	E_p (Pa)	ν_p	ρ_p (kg/m ³)	η	d_{31} (m/V)	ϵ_{33}^T (F/m)
28e-6	5.4e9	0.18	1780	1e-3	23e-12	12 ϵ_0

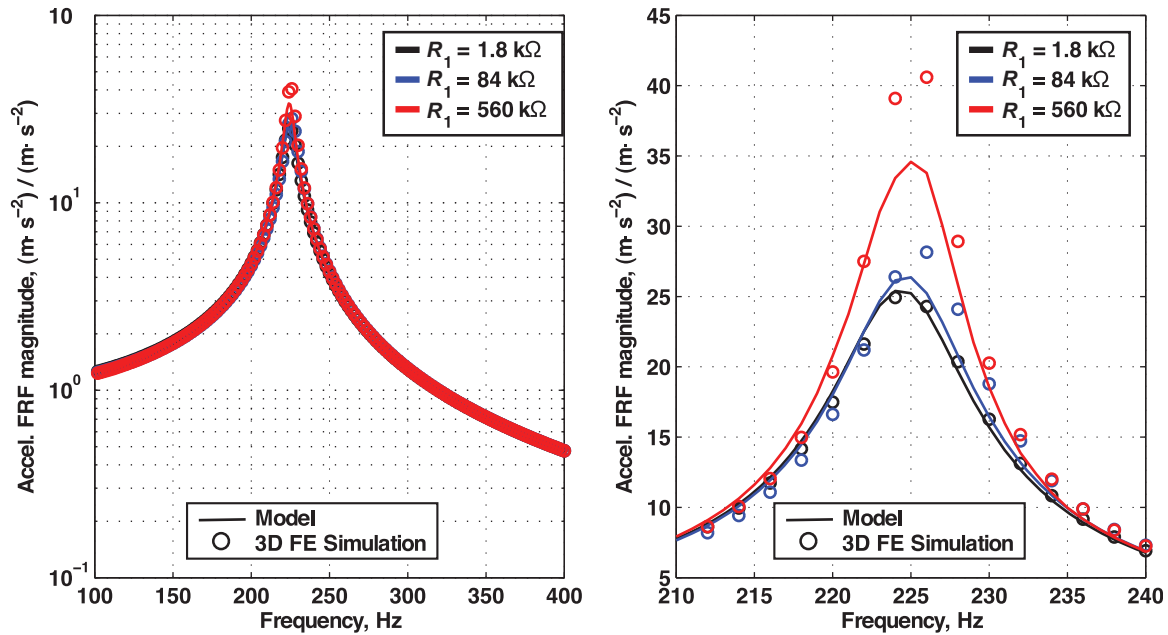


Figure 5. (a) Comparison of acceleration FRF magnitudes for $R_1 = 1.8, 84,$ and $560 \text{ k}\Omega$, full spectrum and (b) around resonance. FRF: frequency response function.

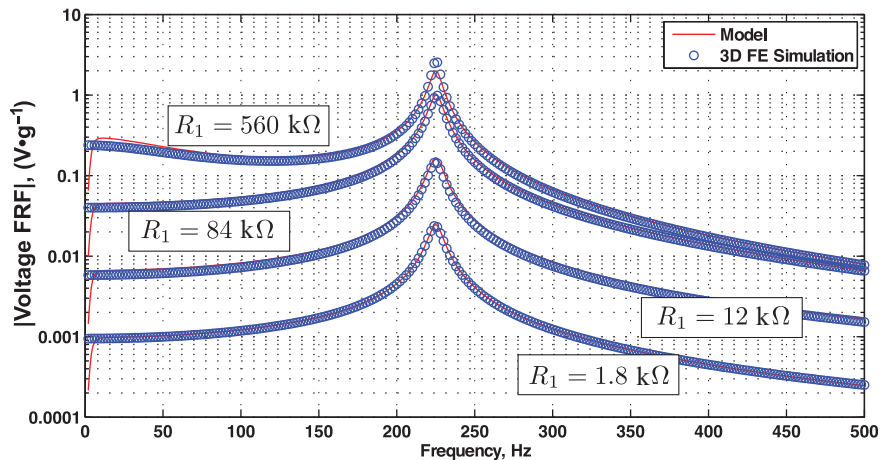


Figure 6. Comparison of voltage FRF magnitudes, solid curves from the present model results and circles from the FE model. FRF: frequency response function; FE: finite element.

components continue to increase. Both models corroborate this feature. Overall, both the 3D FE model and the present numerical model are in close agreement, with a maximum of 15% error (in the acceleration FRF at resonance for $R_1 = 560 \text{ k}\Omega$) but an average error of $<1\%$. To provide a measure of the computational benefit of employing the present continuum domain model, the 2D continuum domain model completed each FRF prediction over 225 times faster than the 3D FE model.

Application: devices on a vibrating panel

Recalling the focus of this work, the goal of the present variational model is to serve as a computationally

efficient means by which to assess and optimize the simultaneous capabilities of passive vibration suppression and power harvesting for distributed piezoelectric devices. To explore some of the utility of the model, consider a clamped plate to which two smart foam devices are attached. The geometry of the model and device layout is shown in Figure 7 with tabulated geometric and mechanical properties in Table 3. As before, the distributed spring layer is considered to have similar isotropic thick plate elasticity parameters. The properties of the embedded piezoelectric film are the same as those provided in Table 2. The plate is excited by an out-of-plane unit point force, $f_z(0.18, -0.16, 0, \omega) = 1 \text{ N}$.

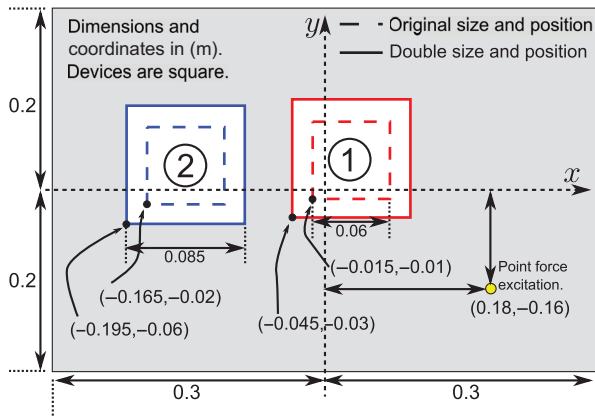


Figure 7. Diagram of modeled geometry and device placement.

Both of the attached devices were square and both were attached to load resistances of $R_1 = 10 \text{ k}\Omega$. Device 1 was designed so as to exhibit a SDOF natural frequency of 141 Hz, very close to the first natural frequency of the clamped panel (144 Hz). Device 2 was designed to have a SDOF natural frequency of 224 Hz, almost identical to the second natural frequency of the panel (223 Hz). The devices were positioned on the panel so as to be most useful in reactively suppressing the vibrations of the clamped panel to which they were tuned.

The out-of-plane mean square velocity of the base plate is computed for three cases: the untreated panel, after attaching the original-sized devices, and for when the areas of the devices were doubled, as in Figure 7. Note that doubling the area of the devices does not alter the SDOF natural frequencies but should, presumably, increase the collective power output of the devices and/or improve vibration-suppression performance. The mass ratio (defined as the total device mass divided by the untreated panel mass) was 2.5%, while doubling the surface coverage of the devices doubled the mass ratio to 5.0%.

Figure 8 plots the mean square velocity of the clamped base plate for the untreated and two additional scenarios with the attached devices. Characteristic of vibration absorbers, the devices significantly reduce the panel vibration at their respectively tuned SDOF natural frequencies, transferring some of the energy to frequencies above and below the untreated panel resonances. Doubling the area of the devices serves to further reduce the magnitude of the split clamped panel resonances around 120 and 157 Hz but does not appreciably reduce the magnitude of the split resonances of

the second mode. However, the added mass does further spread the second mode split resonances away from the untreated resonance, exactly as per the results of classical, analytical treatment of point vibration absorbers (Den Hartog, 1985). Above the devices' SDOF natural frequencies, they do little to suppress the panel vibration; the latter of which almost completely converges to the magnitude of untreated vibration levels by the fourth untreated panel resonance, 427 Hz.

The amplitude of the average power transfer function for the devices

$$P = \frac{|z(\omega)|^2}{2R_1 f_z(\omega)} \quad (12)$$

is plotted in Figure 9. Only one load resistance is considered here, $R_1 = 10 \text{ k}\Omega$, and this may not represent the optimal choice of resistance. However, the important elements to consider are potential trade-offs between vibration-suppression capability and energy-harvesting potential.

From Figure 9, below 300 Hz, it is observed that both devices output greater power around their respective tuned SDOF frequencies, albeit now conforming to the location of the split resonances. From Device 1, greatest power is achieved around the untreated panel resonance at 144 Hz; and from Device 2, greatest power is output around the untreated resonance at 223 Hz. However, since the nature of lightly damped SDOF vibration absorbers is to split the energy around the original, targeted vibrational frequency, the result is that now the absorbers are no longer oscillating at their individual natural frequencies, which would yield significantly greater electrical output.

This issue is perhaps not commonly regarded in most energy-harvesting applications (e.g. transducers to be applied to roadways or bridges) when the mass ratio of the device is negligible compared to the mass of the vibrating structure. In such conditions, the natural frequency of the main structure is not perceptibly shifted and the power-harvesting device oscillates at the designed frequency. In the case of devices designed for simultaneous vibration suppression and energy harvesting, maintaining the lowest mass ratio possible is vital. Otherwise, the resonant frequencies of the host structure are pushed further away from the optimal operating frequency of the energy-harvesting device.

For instance, the doubling of surface coverage of the devices (solid curves in Figure 9) does not noticeably

Table 3. Geometric and mechanical properties of the plate and original-sized devices.

Layer	a (m)	b (m)	h (mm)	E (Pa)	ν	ρ (kg/m ³)	η
Base	0.60	0.40	3	7.1e10	0.33	2100	3e-4
Devices 1 and 2 top	0.06	0.06	2	7.1e10	0.33	2100	3e-4
Device 1 spring	0.06	0.06	75	1.9e5	0.4	9	4e-2
Device 2 spring	0.06	0.06	30	1.9e5	0.4	9	4e-2

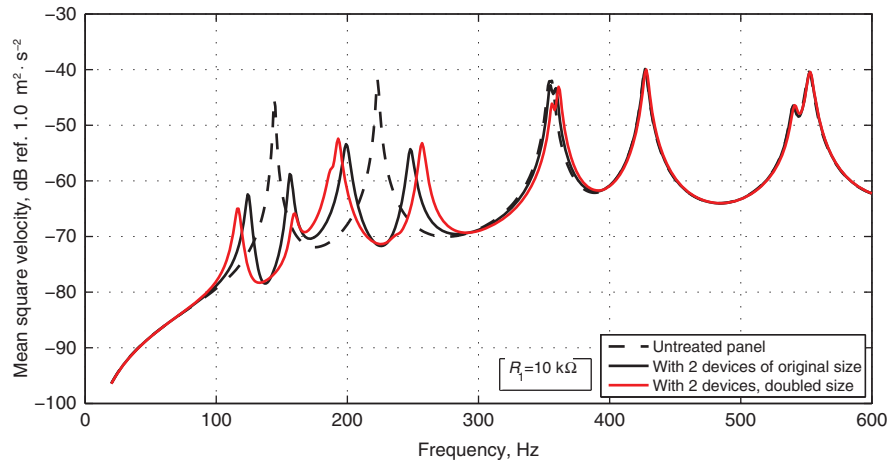


Figure 8. Mean square velocity of untreated panel, with original-sized devices and with double-sized devices.

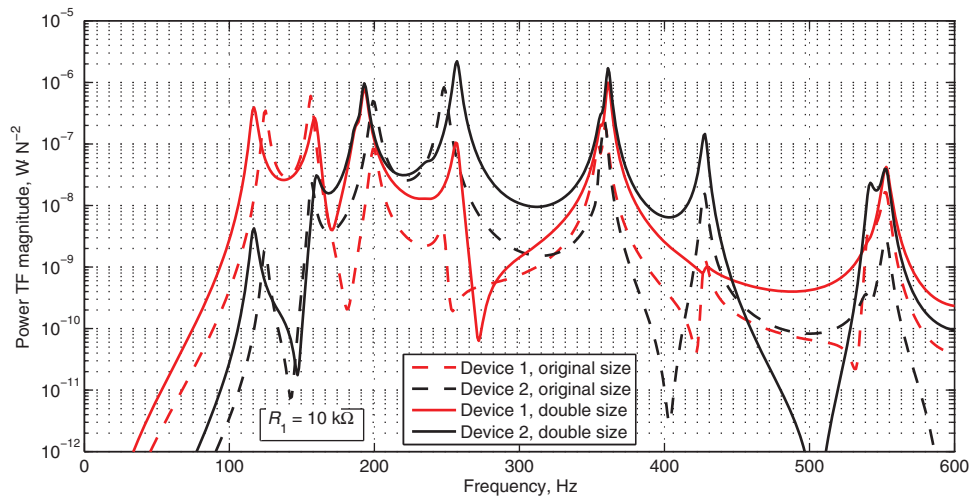


Figure 9. Power of original-sized Devices and of double-sized Devices.

improve the electrical power output, despite a greater volume of piezoelectric material present for charge collection. In fact, Device 1 produces less electrical power at 157 Hz once the area is doubled. Note also from Figure 8 that the vibration of the panel at this frequency is better attenuated with the doubling of size of the devices. Thus, better performance at suppressing the host panel vibration inherently reduces the effectiveness of the device in terms of producing electrical power. This trade-off may be most notably observed by the fact that both devices output an equal or greater amount of power at the third panel resonance, 357 Hz, at which neither of the devices were best designed to operate.

Conclusion

Interest in the capture and conversion of ambient kinetic energy into an electrical power source has

resulted in a wide range of innovative electromechanical and electromagnetic devices. Modeling methods have been equally diverse with the general aim of assisting in the optimization of device design or energy conversion. A variational numerical model was described in this article for the purpose of evaluating the simultaneous reactive vibration-suppression and energy-harvesting capabilities of a class of devices attached to vibrating host structures. Such devices would employ a distributed top mass layer and a distributed spring layer, the latter of which exhibits piezoelectric properties.

The model was compared against a 3D FE model showing close agreement in both mechanical and electrical response of the devices. The model was then employed to evaluate the simultaneous vibration control and power-harvesting potential of similar devices on a clamped panel. Similar to point vibration absorbers, the reactive forcing nature of the device

significantly suppressed the panel vibration at the tuned natural frequencies, splitting the original untreated panel resonances. This result implies that the attached devices no longer oscillate with greatest amplitude at the frequencies to which they would be most useful for energy-harvesting purposes.

Increasing the area coverage of the devices improved the ability to suppress the panel vibration but showed no appreciable improvement in power harvesting, despite the greater volume of piezoelectric material present. While many energy-harvesting devices use an identical, dynamic concept to that of tuned mass-spring-damper systems, the underlying assumption is that the devices are not effective at reducing the vibration of the host structure. Thus, it is assumed that the added mass to the structure is negligible. In the present model, it was observed that for a treatment of devices totaling a 5% mass ratio to the panel mass, a clear trade-off existed between vibration suppression potential and the ability to efficiently convert the remaining kinetic energy into electrical power. The panel resonant frequencies were observed to shift away from the untreated frequencies, as per classical analysis, thereby reducing the effectiveness of the devices since they were tuned to the original, untreated panel resonances.

A few conclusions may be drawn in light of the results:

- The lowest possible mass ratio of the devices to the host structure is important; this reduces the shift in the host panel resonances when tuned reactive devices are attached.
- The devices may improve wider-band vibration suppression by means of improved mechanical coupling to the structure. Extensionally stiffer spring layers may help to improve global vibration reduction performance by means of constraining layer-type effects, while still providing for energy-harvesting capabilities from transverse vibration response.
- The use of more electromechanically coupled piezoelectric materials within the distributed spring layer should yield improved power output. Alternatively, using a greater volume of lightweight piezoelectric film, as in a multitude of periodic film shapes (Figure 2), may achieve similar results.
- For improved energy harvesting, by further study, it may be determined that the devices should be designed so as to exhibit SDOF natural frequencies not exactly equal to the host structural resonances since this reduces the disparity between the split host panel resonances and the original device natural frequency.

While passive, reactive vibration-suppression and energy-harvesting techniques may be important goals to achieve simultaneously, the optimal design of devices

or systems for this purpose will involve the careful assessment and weighing of the inherent trade-offs.

Acknowledgement

The authors are grateful for the continued support of Newport News Shipbuilding and technical monitor Kevin Smith.

Funding

This study was funded by Kevin Smith, Technical Monitor at Newport News Shipbuilding.

References

- Bailo K, Brei D and Grosh K (2003) Investigation of curved polymeric piezoelectric active diaphragms. *Journal of Vibration and Acoustics* 125: 145–154.
- Bakhvalov N and Panasenko G (1989) *Homogenization Averaging Processes in Periodic Media*. Kluwer Academic Publishers, Boston, MA.
- COMSOL AB Inc (2007) *COMSOL Multiphysics User's Guide*. Burlington, MA: COMSOL AB.
- De Marqui C Jr, Erturk A and Inman D (2009) An electromechanical finite element model for piezoelectric energy harvester plates. *Journal of Sound and Vibration* 327(1): 9–25.
- De Marqui C Jr, Erturk A and Inman D (2010) Piezoaeroelastic modeling and analysis of a generator wing with continuous and segmented electrodes. *Journal of Intelligent Material Systems and Structures* 21: 983–993.
- Den Hartog J (1985) *Mechanical Vibrations*. 4th ed. New York: Dover Publications.
- Erturk A, Renno J and Inman D (2009) Modeling of piezoelectric energy harvesting from an L-shaped beam-mass structure with an application to UAVs. *Journal of Intelligent Material Systems and Structures* 20: 529–544.
- Gentry C, Guigou C and Fuller C (1997) Smart foam for applications in passive-active noise radiation control. *Journal of the Acoustical Society of America* 101(4): 1771–1778.
- Guigou C and Fuller C (1999) Control of aircraft interior broadband noise with foam-PVDF smart skin. *Journal of Sound and Vibration* 220(3): 541–557.
- Jacquot R and Foster J (1977) Optimal cantilever dynamic vibration absorbers. *Journal of Engineering for Industry* 99: 138–141.
- Jaouen L, Renault A and Deverge M (2008) Elastic and damping characterizations of acoustical porous materials: available experimental methods and applications to a melamine foam. *Applied Acoustics* 69: 1129–1140.
- Lefevre E, Badel A, Richard C, et al. (2006) A comparison between several vibration-powered piezoelectric generators for standalone systems. *Sensors and Actuators A: Physical* 126: 405–416.
- Leroy P, Atalla N and Berry A (2009) Three dimensional finite element modeling of smart foam. *Journal of the Acoustical Society of America* 126(6): 2873–2885.
- Leroy P, Berry A, Herzog P, et al. (2011) Experimental study of a smart foam sound absorber. *Journal of the Acoustical Society of America* 129(1): 154–164.
- Lesieutre G, Ottman G and Hofmann H (2004) Damping as a result of piezo-electric energy harvesting. *Journal of Sound and Vibration* 269: 991–1001.

Liang J and Liao W (2009) Piezoelectric energy harvesting and dissipation on structural damping. *Journal of Intelligent Material Systems and Structures* 20: 515–527.

Marcotte P, Fuller CR and Cambou P (1999) Control of the noise radiated by a plate using a distributed active vibration absorber (DAVA), in ACTIVE99, December 02-04, 1999. In: *Proceedings of the international symposium on active control of sound and vibration*, Fort Lauderdale, FL, pp.447–456.

Meirovitch L (1967) *Analytical Methods in Vibrations*. Macmillan, New York.

Reddy J (1984) *Energy and Variational Methods in Applied Mechanics: With an Introduction to the Finite Element Method*. New York: Wiley.

Roundy S and Wright P (2004) A piezoelectric vibration based generator for wireless electronics. *Smart Materials and Structures* 13: 1131–1142.

Stephen N (2006) On energy harvesting from ambient vibration. *Journal of Sound and Vibration* 293: 409–425.

Appendix I

Components of equation (6)

The admittance of a circuit attached to the energy-harvesting device is Y^c ; for a single resistive load, R_1 , in the circuit, $Y^c = 1/R_1$.

The capacitance of the piezoelectric layer, $C_p = [A_p(\epsilon_{33}^T - d_{31}^2 E_p)]/t_p$, is a function of A_p , the area of the electrodes; ϵ_{33}^T , the permittivity matrix component evaluated at constant stress; d_{31} , the piezoelectric constant; E_p , the Young’s modulus of the piezoelectric material; and t_p , the thickness of the piezoelectric material.

The superscript t denotes the matrix transpose operator. Note that the piezoelectric thin shell layer requires a change of coordinates in the following equations, to convert from the local, cylindrical system to the global system.

$$\mathbf{K} = \sum_{i=b,s,p,t} \int_{V_i} (\mathbf{L}_u \Psi_m(\mathbf{x}))_i^t \mathbf{c}_i^E (\mathbf{L}_u \Psi_m(\mathbf{x}))_i dV_i \quad (13)$$

$$\mathbf{M} = \sum_{i=b,s,p,t} \rho_i \int_{V_i} (\Psi_m^t(\mathbf{x}))_i (\Psi_m(\mathbf{x}))_i dV_i \quad (14)$$

$$\mathbf{C} = \alpha \mathbf{M} + \beta \mathbf{K} \quad (15)$$

Here, $\alpha = 0$ and $\beta = \eta/\omega$ to employ loss factor damping.

$$\Theta = \int_{V_p} (\mathbf{L}_u \Psi_m(\mathbf{x}))_p^t \mathbf{e}^t \mathbf{L}_v \Psi_v(\mathbf{x}) dV_p \quad (16)$$

$$\mathbf{F} = [\Psi_m^t(\mathbf{x}_{f_1}) \cdots \Psi_m^t(\mathbf{x}_{f_N})] \quad (17)$$

$$\mathbf{e} = \begin{bmatrix} 0 & 0 & 0 \\ 0 & 0 & 0 \\ e_{13} & e_{13} & 0 \end{bmatrix} \quad (18)$$

with components $e_{13} = (d_{31} E_p)/(1 - \nu_p)$

The linear differential operator for the Love–Kirchhoff plates is

$$(\mathbf{L}_u)_{i=b,t} = \begin{bmatrix} \frac{\partial}{\partial x} & 0 & 0 \\ 0 & \frac{\partial}{\partial y} & 0 \\ \frac{\partial}{\partial y} & \frac{\partial}{\partial x} & 0 \end{bmatrix} \quad (19)$$

The linear differential operator for the thick orthotropic plate is

$$(\mathbf{L}_u)_s = \begin{bmatrix} \frac{\partial}{\partial x} & 0 & 0 \\ 0 & \frac{\partial}{\partial y} & 0 \\ 0 & 0 & \frac{\partial}{\partial z_s} \\ 0 & \frac{\partial}{\partial z_s} & \frac{\partial}{\partial y} \\ \frac{\partial}{\partial z_s} & 0 & \frac{\partial}{\partial x} \\ \frac{\partial}{\partial y} & \frac{\partial}{\partial x} & 0 \end{bmatrix} \quad (20)$$

Due to conventional notation in shell theory, a local coordinate system (x, θ, z_p) is defined for the axial, circumferential, and radial directions, having translational displacements of u, v , and w , respectively. The linear differential operator for the thin cylindrical shell, with radius h_s , in the local coordinate system is

$$\mathbf{L}_u = \begin{bmatrix} \frac{\partial}{\partial x} & 0 & 0 \\ 0 & \frac{1}{h_s} \left(1 - \frac{z_p}{h_s}\right) \frac{\partial}{\partial \theta} & \frac{1}{h_s} \left(1 - \frac{z_p}{h_s}\right) \\ \frac{1}{h_s} \left(1 - \frac{z_p}{h_s}\right) \frac{\partial}{\partial \theta} & \frac{\partial}{\partial x} & 0 \end{bmatrix} \quad (21)$$

Assuming the piezoelectric material is poled through its thickness and that the electric potential varies linearly through the thickness of the material, the corresponding linear differential operator is

$$\mathbf{L}_v = \begin{bmatrix} 0 \\ 0 \\ -\frac{1}{h_p} \end{bmatrix} \quad (22)$$

The stiffness matrices of the Love–Kirchhoff plates and the thin shell are

$$\mathbf{c}_{i=b,p,t}^E = \begin{bmatrix} \frac{E_i}{1-\nu_i^2} & \frac{\nu_i E_i}{1-\nu_i^2} & 0 \\ \frac{\nu_i E_i}{1-\nu_i^2} & \frac{E_i}{1-\nu_i^2} & 0 \\ 0 & 0 & \frac{E_i}{2(1+\nu_i)} \end{bmatrix} \quad (23)$$

For the thick orthotropic plate, the stiffness matrix is expressed as

$$\mathbf{c}_s^E = \begin{bmatrix} \frac{1}{E_x} & -\frac{\nu_{yx}}{E_y} & -\frac{\nu_{zx}}{E_z} & 0 & 0 & 0 \\ -\frac{\nu_{xy}}{E_x} & \frac{1}{E_y} & -\frac{\nu_{zy}}{E_z} & 0 & 0 & 0 \\ -\frac{\nu_{xz}}{E_x} & -\frac{\nu_{yz}}{E_y} & \frac{1}{E_z} & 0 & 0 & 0 \\ 0 & 0 & 0 & \frac{1}{G_{yz}} & 0 & 0 \\ 0 & 0 & 0 & 0 & \frac{1}{G_{xz}} & 0 \\ 0 & 0 & 0 & 0 & 0 & \frac{1}{G_{xy}} \end{bmatrix}^{-1} \quad (24)$$